

**3D MEDICAL IMAGE CODING
USING SEPARABLE 3D WAVELET DECOMPOSITION AND
LATTICE VECTOR QUANTIZATION**

Hugues Benoit-Cattin, Atilla Baskurt, Francis Turjman and Rémy Prost

CREATIS

CNRS Research Unit (UMR 5515), affiliated to INSERM

Lyon, FRANCE

submitted to

Signal Processing

Special Issue on Medical Image Compression

This work is supported by PHRC (Programme Hospitalier de Recherche Clinique)

Title : 3D medical image coding using separable 3D wavelet decomposition
and lattice vector quantization

Running head: 3D medical image coding using wavelets

Number of manuscript pages: 20

Number of tables: 2

Number of figures: 13

Corresponding author : Atilla Baskurt

Mailing address: CREATIS, URA CNRS 1216
INSA 502, 69621 Villeurbanne Cedex,
France

e-mail : atilla.baskurt@creatis.insa-lyon.fr

Abstract

An original 3D subband coding scheme is proposed. A separable 3D wavelet, taking full advantage of the 3D structures correlation, decomposes the original volume into subvolumes which can be separately quantized by an uniform scalar quantizer or by a 3D lattice vector quantizer. Concentric hyper-pyramids lying on the cubic lattice are used for searching codewords. A distortion minimization algorithm both selects the best number of decomposition and the best set of quantizers in order to minimize the overall mean square error. The whole algorithm is applied on a 3D image data base issued from the Morphometer (a new true 3D X-Ray scanner). The results presented include traditional signal to noise ratio performances and a subjective evaluation made by radiologists.

Keywords: 3D image coding, wavelet transform, 3D X-ray scanner, bit allocation, scalar quantization, pyramidal vector quantization.

Résumé

Un schéma original de compression sous-bande 3D est proposé. Une décomposition avec une transformation en ondelettes 3D séparable, prenant en compte la corrélation dans les trois directions, est appliquée sur des volumes. Les sous-volumes obtenus sont quantifiés indépendamment par un quantifieur scalaire uniforme ou par un quantifieur vectoriel sur treillis. La recherche des mots-codes se fait à l'intersection d'un ensemble d'hyper-pyramides concentriques avec le treillis cubique. Un algorithme minimisant l'erreur quadratique globale pour un débit imposé permet de sélectionner le nombre de décompositions et d'allouer le meilleur ensemble de quantifieurs aux différents sous-volumes. L'algorithme de codage a été appliqué sur une base de volumes issus du Morphomètre (un vrai scanner 3D à rayon X). Les résultats obtenus en terme de rapport signal sur bruit ainsi que les résultats d'une évaluation subjective effectuée par des radiologues.

1 Introduction

In medical images, 3D images are generally provided by MRI or CT scanners. However, these techniques do not offer the spatial resolution needed in some specific applications, i.e. cardio-vascular imaging. The new true 3D X-Ray scanner, a prototype called "Morphometer" produces discrete volumes up to 512^3 voxels coded on 12 bits with 356 microns of spatial resolution in each direction. The amount of data to store and to transmit is prohibitive when a 3D sequence is acquired using such a system. Thereby, the storage gain which can be provided by dedicated compression algorithms is particularly attractive.

Different approaches may be considered for 3D image compression. Since lossless compression approaches result in a small compression ratio, we consider lossy compression techniques. Several studies dealing with lossy compression of 2D medical images has been proposed and applied to different image modalities (Resonance Magnetic Nuclear Images, Computed Tomography, X-Ray images, ...). Among the main approaches developed, we can note :

- methods using 2D transforms like Discrete Cosine Transform applied to blocks [14,23] or to the whole image [8, 35];
- methods using Tree Structured Vector Quantization [12, 29];
- methods using subband decomposition [1, 21].

One can find complementary references on radiological image compression in [40].

In 3D case, many approaches, closed to the MPEG standard [18], using block matching algorithm for motion estimation has been developed [20, 24] to code medical 2D sequences as numerical angiographies. Such algorithms are not adapted to the compression of real 3D medical images because of the artefacts introduced when quantizing the third dimension which are not acceptable for static data. The 3D Cosine Transform has also been tested on medical sequences [4, 9].

Concerning 3D medical images coding, a subband decomposition using mono-dimensional filter banks associated to a scalar quantizer is proposed in [28, 38, 39]. More recently, a 3D zerotree quantizer has been associated to such a subband decomposition [26]. Such a decomposition takes advantage of the voxel correlation in the three directions. Moreover, as the volumes issued from the Morphometer described in section 2 are isotropic, separable wavelet filter banks is well adapted to this image modality.

In this study, we present an original coding scheme based on a separable 3D wavelet transform associated to both a scalar quantizer and a lattice vector quantizer. Preliminary results of this work have already been presented [5]. Section 2 describes the Morphometer system, its performances and its applications. Section 3 deals with the wavelet transform and its extension to the 3D case. A complete coding scheme, including a very efficient bit allocation procedure is proposed in section 4. Finally section 5 presents results on the volumes issued from the Morphometer.

2 3D Morphometer

The Morphometer [33] is a new true 3D X-ray scanner system installed at the Neuro-Cardiological Hospital of Lyon (Fig. 1). The main goals of this pilot project supported by the French government are:

- to validate new concepts of examinations on humans using 3D X-ray data;
- to optimize the acquisition model function of an examined organs;
- to develop new reconstruction algorithms.

The Morphometer acquires a set of 2D digital projections using two X-ray imaging chains mounted on a modified CT gantry. The rotation speed of the gantry around the patient is 4 to 20 seconds per rotation cycle and provides up to 25 images per second of acquisition. The 2D projections are processed towards the reconstruction algorithms [32, 37] and the reconstructed 3D image is displayed with a dedicated software. The system can generate up to 512^3 discrete volumes with isotropic voxels of 356 microns, each voxel coded on 12 bits. The Morphometer presented in Fig. 2 is divided in four subsystems:

- the modified CT gantry and a bed with four degrees of freedom;
- the acquisition part including two x-ray tubes, two amplifiers, a biplane x-ray generator and the digitization unit;
- the control unit administrating the real time tasks, i.e. the gantry and bed movements and controlling the peripherals in the examination room;
- the processing part including the 3D reconstruction computer and a 3D display station.

Using a standard 3D Computerised Angiography protocol, an examination consists in acquiring the mask images when rotating one way and the opacified images the other way. The injection of contrast agent begins automatically with the inversion of the rotation. 3D reconstruction is processed using the 2D difference image set.

The Morphometer supports several acquisition and reconstruction protocols associated with different medical applications: 3D Computerised Angiography [34] (CA) with one or several injections for neurology (see Fig. 3b), 3D CA gated on ECG for coronarography (Fig. 3a) and also 3D non-vascular applications (bones, articulations, analysis of soft tissues).

The Morphometer offers very important advantages compared to the usual scanners: The image quality is increased . The spatial resolution is higher (356 microns) and equal in the three directions. The examination duration (10 sec. to 40 sec.), the X-ray dose and the quantity of injected contrast agent are considerably reduced.

The proposed coding scheme based on a separable wavelet transform and on the use of independent quantizers and bit allocation with the Ramchandran algorithm [30] is well adapted for the 3D data issued from the Morphometer. It takes into account the constraints and typical properties of the application considered:

- the voxels are isotropic in the three directions. This imposes to consider the same methodology in each direction, like a separable wavelet transform;
- the blocking effects appearing for example in DCT block coding have to be avoided, particularly for angiographies;

- the volumes issued from the Morphometer represent different medical applications like coronarographies, cerebral vessels or bones. The coding scheme has to adapt itself to these changing properties. For a given bit budget, our approach detailed in sections 3 and 4 finds the best quantizer and bit allocation for each subband. Any subband is a priori eliminated. The depth of the wavelet decomposition also changes and adapts itself to the applications and to the volume size (128^3 , 256^3 or 512^3).

3 3D wavelet transform

The continuous wavelet transform of a monodimensional signal $f(x)$, provides a decomposition of the signal at different scales [13]. It is based on the use of an analyzing wavelet $\psi(x)$ which is translated and scaled. The properties of the continuous wavelet transform relies on those of the chosen analyzing wavelet. When this later satisfies a so-called admissibility property, the transform is reversible and the signal may be recovered as a sum of the scaled and translated wavelets weighted by the wavelet coefficients.

The discrete wavelet transform may be interpreted as a decomposition of the signal at different levels of resolution via multiresolution analysis [27] and can be implemented recursively by using a pair of discrete filters via an analysis/synthesis scheme as given in Fig. 4.

In such an approach, a signal at a resolution 0 named a_0 is decomposed into two low resolution signals, an approximation signal a_{-1} and a detail signal d_{-1} , using a low-pass filter (Ba) and a high-pass filter (Ha) respectively, followed by a 2 to 1 decimation. At each resolution j , the decomposition could be repeated on the approximation signal a_j to get a_{j-1} and d_{j-1} (Fig. 4). Finally the wavelet decomposition of the original signal a_0 is given by the approximation signal a_K at the lowest resolution K and all the details signal d_j . Note that the approximation signal a_j at a resolution j and the detail signal d_j at the same resolution are orthogonal due to the fact that they represent the decomposition of the signal a_{j+1} on a wavelet orthonormal basis. A residual correlation still exists between the approximation signal and the details signals. However in our approach detailed in section 4, we propose to use "separate quantizers" in order to have simplicity (independent quantizers) and flexibility (the possibility

of using any kind of quantizer). After coding/decoding, the signal is reconstructed using the contributions of all details signals at the different resolutions and the approximation signal at the lowest resolution. The reconstructed signal \hat{a}_{j+1} is calculated by a 1 to 2 upsampling of a_j and d_j and by a filtering with the low-pass (Br) and the high-pass (Hr) interpolating filters (Fig. 4). In the Z transform domain, the previous operations result in:

$$\hat{A}_{j+1}(z) = 1/2.[Ba(z).Br(z) + Ha(z).Hr(z)].A_{j+1}(z) + [Ba(-z).Br(z) + Ha(-z).Hr(z)].A_{j+1}(-z) \quad (1)$$

In this equation, the first term contains the frequency response of the decomposition-reconstruction system and the second one corresponds to the aliasing terms. By imposing conditions on filters Ba, Ha, Br and Hr, perfect reconstruction is achieved, then $\hat{A}_{j+1}(z)=A_{j+1}(z)$ and the decomposition/reconstruction is free of aliasing and free of module distortion. Many solutions have been proposed to achieve the perfect reconstruction [13, 22, 36]. Recent studies [7, 31] have shown that these solutions lead to very similar coding performances. In the 3D coding scheme we proposed, Daubechies orthonormal wavelets CQF [13] have been implemented.

The wavelet transform has been extended [41] to images, by applying separately the analysis/synthesis scheme on the rows and then on the columns. When using a separable 2D analysing wavelet, each decomposition level provides four subimages, a low resolution subimage and three subimages of details. Coding scheme based on such an approach leads to interesting performances compared to standardized compression algorithms [2, 6].

In the same way, 3D wavelets can be constructed as separable products of 1D wavelets by successively applying a 1D analyzing wavelet in three spatial directions (x,y,z). Fig. 5 shows a separable 3D decomposition of a volume: after being applied on the rows and on the columns, the analysis/synthesis filters followed by a 2 to 1 decimation are applied along the third dimension. At the end of the decomposition, 8 subvolumes of lower resolution are obtained: the approximation subvolume from resolution '-1' named LLL1 and 7 subvolumes of details. The separable 3D wavelets will provide an equal decorrelation of the original volume voxels in the three directions. All the subvolumes can be separately quantized and coded.

4 3D subband coding scheme

The separable 3D wavelet decomposition has been implemented in the coding scheme presented in Fig. 6. We first describe the quantizers developed for this scheme. Then we detail the bit and quantizer set allocation algorithm.

4.1 Quantizers

Uniform Scalar Quantizer (USQ)

USQ transforms the original voxel (v) in an integer value (q) scaled between 0 and 2^B-1 with B a given coding rate in bit per pixel (bpp) using the linear equation

$$q = \text{round}(a \cdot v + b) \quad (2)$$

where a and b are reals and both depend of the original voxel dynamic and of the given coding rate B . The reconstructed voxel (\hat{v}) is given by

$$\hat{v} = (q - b) / a \quad (3)$$

Quantized data is entropy coded using a Huffman coder.

Pyramidal Vector Quantizer (pyramidal VQ)

The rate distortion theory and several studies [15, 19, 42] have underlined the superiority of vector quantizer over scalar quantizer especially on highly correlated images which are encoded at a low bit rate.

The basic idea of vector quantizers is to quantize pixel sequences rather than single pixels. Each original vector (block of pixels) is quantized with the nearest (using a distance criteria) vector belonging to a codebook. The codebook size is equal to 2^{BN} where B corresponds to the desired bit rate and N to the vector dimension. The first vector quantization algorithm has been proposed by Lind Buzo Gray (LBG) [25]. Although this algorithm is able to provide a locally optimal codebook for a given image, it has two major drawbacks: it is clear that for a large vector dimension N or for a high coding rate B , the VQ complexity grows exponentially because the codewords have to be chosen between 2^{BN} possible vectors.

In order to avoid LBG disadvantages, the codebook of the vector quantizer we use corresponds to a lattice subset. A lattice can be simply defined as a regular set of points in a N dimensional space \mathcal{R}^N . The lattice properties have been investigated by Conway et al. [10] which have determined the optimal lattices for several dimensions. The quantization of a

vector X consists in finding the closest lattice point Y to X . This search becomes extremely fast when using quantizing algorithm proposed by Conway et Sloane [11].

The lattice vector quantizer has been initially investigated for uniform and Gaussian distributions under the name of Spherical Vector Quantizer (SVQ) [11]. Pyramidal Vector Quantizer (pyramidal VQ) has been proposed by Fischer [16, 17] for the quantization of images with Laplacian and generalized Gaussian distributions and applied in a multiscale image coding scheme [3]. The main differences between SVQ and pyramidal VQ lie in the norm used to compute vector energy: L_2 and L_1 norm for SVQ and for pyramidal VQ respectively. This norm also determines a set of hyper-surfaces: hyper-sphere and hyper-pyramid for SVQ and pyramidal VQ respectively. Vectors lying on a given hyper-surface have the same energy.

In this study, taking into account the Laplacian distribution of high frequency subbands, we develop a 3D Pyramidal Vector Quantizer using vector of $2 \times 2 \times 2$ pixels. Note that vector energy E_X is computed using L_1 norm as follows:

$$E_X = \sum_{i=1}^2 \sum_{j=1}^2 \sum_{k=1}^2 |X(i, j, k)| \quad (4)$$

where $X(i,j,k)$ is a gray level. The following algorithm is used for quantization and coding:

a) For a given bit rate B , find the radius (energy) E such that the hyper-pyramid of radius E includes at least $2^{8 \times B}$ lattice points. The points of the lattice subset delimited by this pyramid correspond to the possible codebook vectors. They all lie on hyper-pyramids of integer radius. Using the formula proposed by Fischer [16]:

$$\text{Num}(N,K) = \text{Num}(N-1,K) + \text{Num}(N-1,K-1) + \text{Num}(N,K-1) \quad (5)$$

we find the number of lattice points $\text{Num}(N,K)$ lying on a hyper-pyramid of radius K in \mathcal{R}^N . Adding $\text{Num}(N,K)$ for successive concentric hyper-pyramids, we obtain E .

b) Fix the maximum of energy E_M to be encoded. This energy can differ from the energy of the most energetic vector (E_{\max}). Indeed, taking E_M under E_{\max} allows a better

quantization of low energetic vector (limiting the risk of being quantized to 0 in \mathbb{R}^8) and also a specific quantization of few high energetic vectors.

c) Scale each vector into the hyper-pyramid of radius E using a scaling factor (Fig. 7):

- X_1 , vector of energy lower than E_M , scaled by $A = \frac{E_M}{E}$;
- X_2 , vector of energy equal to E_M , scaled by A . As $A = \frac{E_M}{E} = \frac{E_{X_2}}{E}$, the scaled X_2 lies on the hyper-pyramid of radius E ;
- X_3 , vector of energy greater than E_M , scaled by a proper scaling factor α given by $\alpha = \frac{E_{X_3}}{E}$.

d) Each scaled vector is projected onto the nearest hyper-pyramid of integer radius and the nearest cubic lattice point is found on the hyper-pyramid;

e) An enumeration procedure [17] allows us to associate an integer to each quantized vector. Taking into account the Gaussian distribution of the quantized vectors radius, we encode the radius E_X using an Huffman table. Note that this Huffman table includes an additional code for vectors of X_3 type. This code is computed regarding the cumulative probability of these vectors. Finally, scaling factor A and α are quantized with 8 bits, their values do not exceed 255.

The decoding process is very simple:

- a) Decoding the radius E_X and the enumeration index gives the lattice point.
- b) To expand the vectors, we use (Fig. 7):

- $\frac{1}{A}$ if $E_X \leq E_M$, case of X_1 and X_2 type vectors;
- $\frac{1}{\alpha}$ if we get the additional code (X_3 type vectors with $E_X > E_M$)

Note that the specific quantization of few X_3 type vectors provides an interesting quality gain for a negligible bit rate cost.

4.2 Distortion Minimization Algorithm (DMA)

This algorithm has been proposed [30] for 2D image coding using wavelet packets which differ from wavelets decomposition by the fact that even the detail subimages are

recursively decomposed. DMA selects the best quantizers (the bit allocation and the quantizer for each subimage) in the set of quantizer proposed and the best number of decompositions in order to minimize the overall mean square error (D) under the constraint of a total number of coding bits (R) lower than a coding bit budget (R_b). This is a minimization problem under a constraint given by

$$\underset{R \leq R_b}{\text{Min}}(D) \quad (6)$$

Using the additivity properties of the rate and the distortion over one step of decomposition [30] provided by using orthonormal filters, the constraint problem (6) is treated by an unconstrained optimization procedure using a Lagrangian cost function J which merges the rate and the distortion in the Lagrangian multiplier λ . J is defined by

$$J = D + \lambda R \quad (7)$$

Let us describe the main steps of DMA:

a) N_q possible quantizers (quantization and coding) and a maximum number of decompositions N_d are fixed.

b) The volume to encode is decomposed N_d times. Each decomposition provides 8 subvolumes. Thus the total number of subvolumes (N_{sb}) to work with, is given by ($8 \times N_d$). DMA really begins at step c).

c) The original volume and the N_{sb} subvolumes are quantized separately by all the N_q quantizers. Each time, the local distortion (D_{ijk}^j) induced by the k^{th} quantizer on the i^{th} subvolume at resolution j is computed as well as the resulting number of coding bits R_{ijk}^j .

d) Then DMA calls successively two procedures:

- *Procedure 1* searches, for a given λ , the best decomposition and the best set of quantizers in order to minimize the total Lagrangian cost J. This could be written as

$$\underset{q_k}{\text{Min}}(J) = \underset{q_k}{\text{Min}}(D + \lambda R) = \sum_i \underset{q_k}{\text{Min}}(D_i + \lambda R_i) \quad (8)$$

This procedure is easy to implement. Indeed, for each subvolume i of a resolution j, it searches the quantizer which minimizes the local Lagrangian cost J_i^j . If the sum of all the Lagrangian costs at a resolution j is greater than the Lagrangian cost of the approximation subvolume at the upper resolution j+1, which is formulated as follows

$$J^j = \sum_{i=0}^7 J_i^j = \sum_{i=0}^7 D_i^j + \lambda R_i^j > J_0^{j+1} \quad (9)$$

then the decomposition tree is pruned of the resolution j and thus the best level of decomposition becomes $(j+1)$.

- *Procedure 2* searches the optimal Lagrangian multiplier λ_{opt} , which assumes $R \leq R_b$. The Lagrangian multiplier λ equal to λ_{opt} is in fact the solution of the following problem:

$$\text{Max}_{\lambda} [D(\lambda) + \lambda(R(\lambda) - R_b)] \quad (10)$$

This maximization procedure is done by a Newton algorithm [30] which quickly converges to the optimal point $(R_{\text{opt}}, D_{\text{opt}})$ with $(R_{\text{opt}} \leq R_b)$.

Both procedures are illustrated on Fig. 8. Plotting all the possible (R, D) points, coming from all the combinations (R_{ik}^j, D_{ik}^j) leads to a cluster on the (R, D) plan. The optimal solution $(R_{\text{opt}}, D_{\text{opt}})$ is on the convex hull of the cluster. In fact *Procedure 1* searches the first intersection between a line of slope $-\lambda$ and the convex hull. On Fig. 8, point A corresponds to the intersection with the line of slope $-\lambda_1$. *Procedure 2* searches λ_{opt} which maximizes the y -coordinate of the intersection between the line of slope $-\lambda_{\text{opt}}$ and the vertical line of x -coordinate R_b . Point I corresponds to this intersection on Fig. 8: y -coordinate of I is equal to $D + \lambda(R - R_b)$.

For easy visualization, a 2D example of bit allocation with DMA is presented in Fig. 9. DMA decomposes Lena 512x512x8 until level 3 with 8 taps Daubechies FIR filters. 2x2 blocks are used for pyramidal VQ. The given bit budget is 1 bpp. The PSNR after reconstruction is 36.1 dB.

Note that DMA algorithm selects the best wavelet decomposition depth which depends on the image to be encoded and on the image modality considered. This way, our algorithm is fully adaptive to the different image modalities (vessels, bones,...) and to the image size (128^3 to 512^3). In Fig. 10, we present PSNR/bpp curves on Lena 512x512x8 showing an example of the gain obtained by adapting the scale versus keeping a fixed scale.

5 Results

In this section we present results obtained on an image data base issued from the Morphometer. The volumes are encoded with the coding scheme described in section 4. The maximum number of decompositions has been fixed to 3. So 2 bits are necessary to code the resolution j , varying from 0 (original image) to 3. The subvolume number i is also coded with 3 bits for a given resolution. Finally, 1 bit is used to distinguish the selected quantizer: uniform scalar quantizer or pyramidal vector quantizer. The wavelet decomposition is performed using 8 taps, approximately linear phase and orthonormal wavelet filter of Daubechies [13] with a circular convolution. The set of possible quantizers is constituted with 19 USQ corresponding to bit rates from 1 to 9 bpp with a 0.5 bpp step and 9 pyramidal VQ from 1 to 5 bpp with the same step. Note that for pyramidal VQ, we use $2 \times 2 \times 2$ blocks. This corresponds to varying the radius of the bounded space in \mathfrak{R}^8 to obtain lattices containing from 2^8 to 2^{40} points. Both original 128^3 volumes and 128^3 ROI in 256^3 volumes have been treated with our algorithm.

Table 1 and Table 2 present the bit and quantizer allocation realized using DMA on the coronarography of Fig. 3a. In Table 1, DMA uses only USQ for a given bit budget of 0.8 bpp and gives PSNR = 40dB. In Table 2, USQ and pyramidal VQ are possible quantizers for DMA. High frequency subbands (specially the resolution "-1") are quantized with pyramidal VQ at low bit rates. Indeed, pyramidal VQ allows to go down in bpp and remains the most performant quantizer until about 1.7 bpp. USQ is chosen when DMA allocates more than about 1.9 bpp. Combining two quantizers, PSNR is increased to 44.7dB for the same bpp (0.8 bpp). This analysis has been validated with several experiments done on the image data base. Fig. 11a shows the decoded 3D coronarography after Table 2 allocation and after reconstruction (0.8 bpp, PSNR = 44.7 dB). The quality is very satisfying when compared with the original image (Fig. 3a). Fig. 11b presents the decoded image associated to Fig. 3b. We obtain PSNR = 40.4 dB for the same bit budget 0.8 bpp.

Fig. 12 presents PSNR/bpp results obtained with an angiography issued from the data base and compares our method to a 3D DCT approach [4]. The results show the limitation of the 3D DCT based algorithm, especially for low bit rates.

As our algorithm has been found efficient using objective criteria (PSNR/bpp), we perform a subjective quality evaluation with radiologists. The results presented have been obtained on a specific Morphometer modality: 3D mini-pig left ventricle angiography. Each volume is coded using 6 bit per pixel rate : 0.1, 0.13, 0.16, 0.2, 0.26 and 0.4 bpp (compression ratios of 80, 60, 48, 40, 30 and 20 respectively). Two blinded experienced senior radiologists were asked to evaluate "the quality of the image for diagnosis purposes". As in [12], five subjective image qualities were distinguished by the allowed responses:

1. Unacceptable quality (image not usable)
2. low quality (image very difficult to use)
3. passable quality (image usable but below standard)
4. good quality (image usable and very adequate)
5. excellent quality (image usable)

The quality evaluation is mainly based on the sharpness of small vessels (internal mammary arteries and the major trunk of the coronary artery), on the quality of the "pig tail" catheter and on the stepping effects. The volumes are visualized on the display station of the Morphometer using the RAO projection. Note that the radiologists can modify lightness and contrast interactively.

The evaluation has been done on 20 volumes of 128^3 voxels. These volumes are all taken from sequences of 3D Coronarography of a mini pig's left ventricle. Each reader evaluated 120 decoded volumes divided in 6 sessions of 20 volumes. In each session, a random sequence is presented without the knowledge of the bit rates. The reader could not go back to review a previous volume. After independent evaluation, the two readers discussed and made the final evaluation in consensus [43, 44]. This leads to a "subjective quality" / bit rate(bpp) curve obtained using a cubic spline interpolation where the 'o' represents the mean score on 20 volumes for a given bit rate. Note that a bit rate with a score under the quality 3 is unacceptable. The curve shows (Fig. 13) that 0.18 bpp rate (compression ratio of 44) seems to be a lower bound giving a usable image quality for diagnosis purposes considering this image modality.

The CPU time on a Silicon Graphics Indigo II station associated to the 3D compression algorithm is 300 seconds for 128^3 volumes with 70 % used by the DMA. It is about 40 seconds for the 3D decompression program. These 3D programs are not optimized in term of runtime. Optimizing the dynamic memory allocation and implementing a fast algorithm for the circular convolution in the 2D case led us to considerably reduce the CPU time needed (8 sec. to 1 sec. for the compression of a $512 \times 512 \times 8$ image on SG Indigo II). The optimization of the 3D programs is under investigation.

One drawback of the approach presented in this paper is the computational time of the DMA. This inconvenient aspect could be removed, by a learning step: indeed for each image modality and for a set of compression rates, the DMA can be used to choose the best quantizer and the best number of decompositions. Then the DMA could be replaced in the coding scheme by parameters chosen during the learning step. This approach avoids to execute the whole "Distortion Minimization Algorithm" for coding an image belonging to the same modality.

6 Conclusion

In this paper, we have proposed an original 3D coding scheme based on 3D wavelet transforms associated with 3D lattice vector quantization and uniform scalar quantization. A Distortion Minimization Algorithm (DMA) selects the best set of quantizers (bit and quantizer allocation) and the best number of decomposition and makes our algorithm fully adaptive to different image modalities. This scheme has been used to code images issued from a real 3D scanner, the Morphometer. The results obtained on an image data base issued from the Morphometer have been presented. The quality of the reconstructed images is significantly improved comparing to a classical 3D DCT approach. For high compression ratios, the signal-to-noise ratios are very satisfactory. A subjective quality evaluation done by two senior radiologists on mini-pig left ventricle angiography volumes has given a lower bound in bpp (0.18 bpp) which gives an acceptable image quality for diagnosis using this image modality. These results urge us to continue the medical evaluations using large data bases and involving 4 or 5 radiologists. The final goal is to determine a bit rate bound for each Morphometer application.

7 Acknowledgment

The authors wish to express their thanks for their active collaborations in the quality evaluation of 3D angiography, to the physicians Pr D. Revel and Pr M. Amiel of the Therapeutic and Diagnostic Imagery Department of Neuro-Cardiological Hospital of Lyon.

8 References

- [1] P. A. Angelidis, "MR image compression using a wavelet transform coding algorithm", Magnetic Resonance Imaging, Vol. 12, N° 7, July 1994, pp. 11-1120.
- [2] M. Antonini, M. Barlaud and P. Mathieu, "Digital image compression using vector quantization and the wavelet transform," in Wavelet and applications, Y.Meyer, Ed. Masson, 1992, pp. 160-174.
- [3] M. Barlaud, P. Sole, T. Gaidon, M. Antonini and P. Mathieu, "Pyramidal lattice vector quantization for multiscale image coding, " IEEE Trans. Image Processing, Vol IP-3, No. 4, July 1994, pp. 367-381.
- [4] A. Baskurt and R. Goutte, "3-dimensional image compression by discrete cosine transform", Proc. Eusipco-88, Grenoble, Sep. 1988, pp. 79-82.
- [5] A. Baskurt, H. Benoit-Cattin and C. Odet, "On a 3D medical image coding method using a separable 3D wavelet transform," Proc. SPIE Medical Imaging IX: Image display, San Diego, California, Feb.1995, Vol. 2431, pp. 173-183.
- [6] H. Benoit-Cattin, O. Baudin, A. Baskurt and R. Goutte, "Coding mammograms using wavelet transform," Proc. SPIE Medical Imaging VIII: Image display, San Diego, California, 1994, pp. 282-290.
- [7] H. Benoit-Cattin, A.Baskurt, F. Peyrin and R. Goutte, "A Study on FIR Filters for Subband Coding of Images," Proc. Eusipco-94, Edinburg, Scotland, Sep. 1994, pp. 1238-1241.
- [8] P. Beretta, R. Prost, "Unsharp masking and its inverse processing integrated in a compression decompression scheme. Application to cardiac angiograms", Proc. SPIE Medical Imaging IX, San Diego, California, Feb. 1995, pp. 233-244.
- [9] V. Chameroy and R. Di Paola, "Compression de séquences d'images médicales", Proc. GRETSI-89, Juan-les-Pins, France, 1989, pp. 961-964.

- [10] J.H. Conway and N.J.A. Sloane, "Voronoi regions of lattices, second moments of polytopes, and quantization," IEEE Trans. on Information Theory ,Vol. IT-28, Mar. 1982, pp. 211-226.
- [11] J.H. Conway and N.J.A. Sloane, "Fast quantizing and decoding algorithms for lattice quantizers and codes," IEEE Trans. on Information Theory ,Vol. IT-28, Mar. 1982, pp. 227-232.
- [12] P. C. Cosman, C. Tseng, R. M. Gray, Olshen R. A., Moses L. E., Davidson H. C., Bergin C. J., Riskin E. A., "Tree structured vector quantization of CT chest scans: Image quality and diagnostic accuracy", IEEE Trans. on Medical Imaging, Vol. 12, No. 4, Dec. 1993, pp. 727-739.
- [13] I. Daubechies, Ten lectures on wavelets, Ed. Society for industrial and applied mathematics, Philadelphia, Pennsylvania, 1992, 357p.
- [14] Y. Ding, O. Baudin, P. Beretta, R. Prost, "Medically adapted JPEG compression scheme", Proc. SPIE Medical Imaging, San Diego, California, Vol. 2431, Feb. 1995, pp. 516-525.
- [15] T.R. Fischer and R.M. Ditcharry, "Vector quantization of memoryless Gaussian, gamma and Laplacian sources," IEEE Trans. on Communication, Vol. COM-32, Sep. 1984, pp. 1065-1069.
- [16] T.R. Fischer, "A pyramid vector quantizer," IEEE Trans. on Information Theory ,Vol. IT-32, july 1986, pp. 568-583.
- [17] T.R. Fischer, "Geometric source coding and vector quantization," IEEE Trans. on Information Theory ,Vol. IT-35, Jan. 1989, pp. 137-145.
- [18] D. Le Gall, "The MPEG video compression algorithm", Signal Processing: Image Communication, Vol. 4, N° 2, April 1992, pp. 129-140.
- [19] R.M. Gray and Y. Linde, "Vector quantizers and predictive quantizers for Gauss-Markov sources," IEEE Trans. on Communication, Vol. COM-30, Feb. 1982, pp. 381-389.
- [20] B. K. T. Ho, P. Saipetch, J. Wei, M. Ma, J. Villansenor, M-J. Tsai, "Video compression algorithm for dynamic angiographic images", Proc. SPIE Medical Imaging, Newport Beach, California, Vol. 2164, Feb. 1994, pp. 302-309.
- [21] W-L. Hsu, H. Derin, "Saptial and frequency decomposition for image compression", Proc. SPIE Medical Imaging, San Diego, California, Vol. 2431, Feb. 1995 ,pp. 623-634.

- [22] J.D. Johnston, "A Filter Family Designed for Use in Quadrature Mirror Filters Bank," Proc. ICASSP-80, 1980, pp. 291-294.
- [23] T. H. Karson, S. Chandra, A. Morehead, S. E. Nissen, J. D. Thomas, "Digital compression of echographic images: is it viable?", Proc. Computers in Cardiology, London, Sept. 1993, pp. 831-834.
- [24] H. Lee, Y. Kim, A. H. Rowbey, E. A. Riskin, "Statistical distributions of DCT coefficients and their application to an interframe compression algorithm for 3D medical images", IEEE Trans on Medical Imaging, Vol. 12, N° 3, Sept. 1993, pp. 478-485.
- [25] Y.L. Linde, A. Buzo and R.M. Gray, "An algorithm for vector quantizer design," IEEE Trans. on Communication, Vol. COM-28, Jan. 1980, pp. 84-95.
- [26] J. Luo, X. Wang, C. W. Chen, K. J. Parker, "Volumetric medical image compression with three dimensional wavelet transform and octave zerotree coding", Proc. SPIE Visual Communications and Image Processing, Orlando, Florida, Vol. 2727, March 1996, pp. 579-590.
- [27] S. Mallat, "A Theory for Multiresolution Signal Decomposition: The Wavelet Representation," IEEE Trans. Patt. Rec. and Mach. Int., Vol. PAMI-11, No. 7, July 1989, pp. 2091-2110.
- [28] A. Manduca A., "Interactive wavelet based 2D and 3D image compression", Proc SPIE Medical Imaging, Newport Beach, Vol. 1897, Feb. 1993, pp. 307-318.
- [29] G. Poggi, R. A. Olshen, "Pruned tree structured vector quantization of medical images with segmentation and improved prediction", IEEE Trans. on Image Processing, Vol. 4, N° 6, June 1995, pp. 734-742.
- [30] K. Ramchandran and M. Vetterli, "Best wavelet packet bases in rate-distortion sense," ", IEEE Trans. on Image Processing, Vol. 2, No. 2, Apr. 1993, pp.160-175.
- [31] O. Rioul, "On the Choice of Wavelet Filters for Still Image Compression," Proc. ICASSP-93, Minneapolis, USA, Apr. 1993, pp. 550-553.
- [32] D. Saint-Félix, Y. Trouset, C. Picard and A. Rougée, "3D reconstruction of high contrast objects using a multi-scale detection/estimation scheme," 3D imaging in medicine, NATO ASI series F60, Berlin:Springer, 1990, pp. 147-158.
- [33] D. Saint-Félix, C. Picard, C. Ponchut, R. Roméas, A. Rougée and Y. Trouset, "Three dimensional x-ray angiography: first in vivo results with a new system," Proc. SPIE Medical Imaging VII, San Diego, California, 1993, pp. 90-98.

- [34] D. Saint-Félix, Y. Troussel, C. Picard, C. Ponchut, R. Roméas and A. Rougée, "In vivo evaluation of a new system for 3D computerized angiography", Journal of Physics in Medicine and Biology, Vol. 39, 1994, pp.583-595.
- [35] J. Sayre, D. R. Aberle, I. Boechat, T. R. Hall, H. K. Huang, B. K. Ho, "Effect of data compression on diagnostic accuracy in digital hand and chest radiography", Proc. SPIE Medical Imaging, Newport Beach, California, Vol. 1653, Feb. 1992, pp. 233-240.
- [36] M.J.T. Smith and T.P. Barnwell, "Exact reconstruction techniques for tree-structured subband coders," IEEE Trans. on Acous. Speech and Sig. Proc., Vol. ASSP-34, No. 3, 1986, pp. 434-441.
- [37] Y. Troussel, D. Saint-Félix, A. Rougée and C. Chardenon, "Multi-scale cone-beam X-ray reconstruction," ", Proc. SPIE Medical Imaging, Newport Beach, California, Vol. 1231, 1990, pp. 229-238.
- [38] J. Wang, H. K. Huang, "Three dimensional medical image compression using a wavelet transform with parallel computing", Proc. SPIE Medical Imaging IX, San Diego, California, Vol. 2431, Feb. 1995, pp. 162-172.
- [39] J. Weil, P. Saipetch, R. Panvar, D. Chen, B. K. T. Ho, "Volumetric image compression by 3D discrete wavelet transform", Proc. SPIE Medical Imaging IX, San Diego, California, Vol. 2431, Feb. 1995, pp. 184-194.
- [40] S. Wong, L. Zarembo, D. Gooden, H.K. Huang, "Radiological image compression : a review", Proc. IEEE, Vol. 83, No. 2, Feb. 1995, pp. 194-219.
- [41] J.W. Woods and S. D. O'Neil, "Subband coding of images, " IEEE Trans. Acous. Speech and Sig. Proc., Vol. ASSP-4, Oct. 1986, pp. 1278-1288.
- [42] Y. Yamada, S. Tazaki and R.M. Gray, "Asymptotic performance of block quantizers with differences distortion measures," IEEE Trans. Inform. Theory , Vol. IT-26, No. 1, Jan. 1980, pp. 6-14.
- [43] PIOPED Investigators, "Value of the ventilation/perfusion scan in acute pulmonary embolism: results of the prospective investigation of pulmonary embolism diagnosis (PIOPED)", JAMA, Vol. 263, 1990, pp. 2753-2759.
- [44] M. Remy-Jardin, J. Remy, F. Deschilde, D. Artaud, J.P. Bergei, C Hossein-Foucher, X. Marchandise, A. Duhamel, "Diagnosis of pulmonary embolism with spiral CT: comparison with pulmonary angiography and scintigraphy", Radiology, Vol. 200, 1996, pp. 699-706.

Captions

- Fig. 1** The CT gantry of the Morphometer at the Neuro-Cardiological Hospital of Lyon.
- Fig. 2** Subsystems of the Morphometer.
- Fig. 3** **3a** Angiography of a pig's left ventricle;
3b Angiography of pig's carotid artery.
- Fig. 4** Wavelet decomposition/reconstruction implemented by using pairs of discrete filters via multiresolution analysis.
- Fig. 5** Separable 3D wavelet decomposition.
- Fig. 6** Coding scheme using separable 3D wavelets.
- Fig. 7** Graphic illustration of the DMA
- Fig. 8** Pyramidal Lattice Vector Quantization of 2D vectors in \mathcal{R}^2 .
- Fig. 9** Example of bit assignment on Lena (512x512x8) for a given bit rate of 1 bpp, using a 8 taps Daubechies FIR (PSNR=36.1 dB at the reconstruction). S and V mean USQ and pyramidal VQ respectively.
- Fig. 10** PSNR(dB)/ bit rate(bpp) curves obtained with Lena 512x512x8 showing the gain obtained by adapting the wavelet transform depth versus keeping a fixed depth (2 and 3).
- Fig. 11** **11a** Angiography of Fig. 3a coded at 0.8 bpp: PSNR= 44.7 dB.
11b Angiography of Fig. 3b coded at 0.8 bpp: PSNR = 40.4 dB.
- Fig. 12** PSNR(dB)/ bit rate(bpp) curves obtained with an angiography issued from the image data base, comparing our method to a 3D DCT approach.
- Fig. 13** Subjective quality evaluation after consensus versus bit rate(bpp): 'o' represents the mean score on 20 volumes; '*' represents the minimum bpp to have usable quality.
- Table 1** Number of bpp allocated by DMA to the subvolumes for a total coding rate of 0.8 bpp on Fig. 3a, using only USQ: PSNR = 40 dB.
- Table 2** Number of bpp allocated by DMA to the subvolumes for a total coding rate of 0.8 bpp on Fig. 3a, using USQ and pyramidal VQ: PSNR = 44.7 dB.

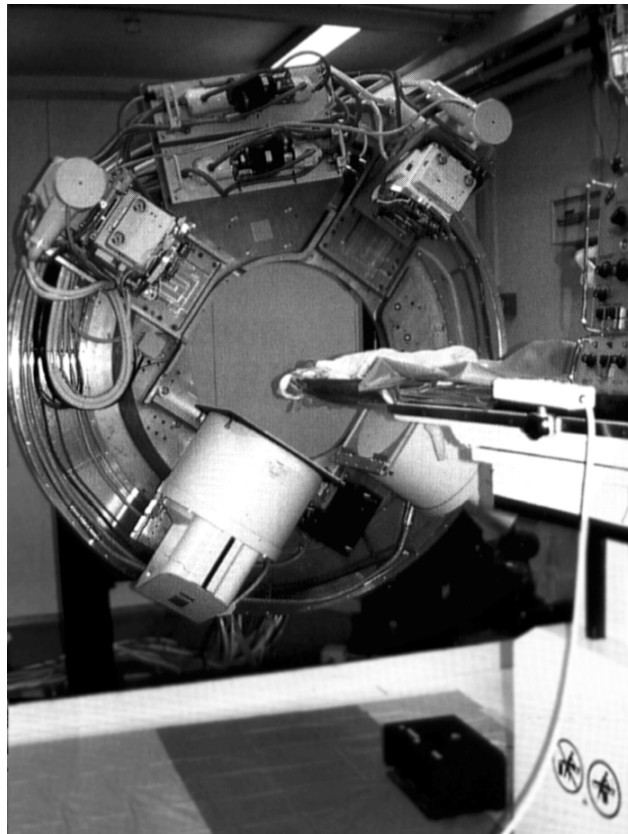


Fig. 1

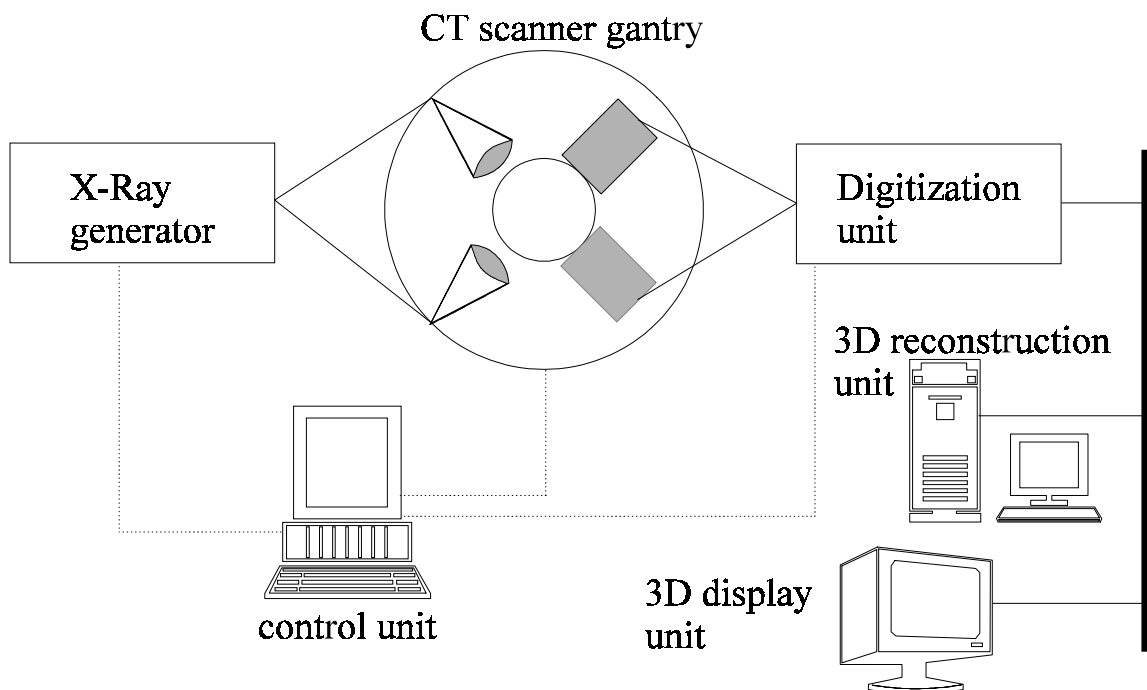


Fig. 2

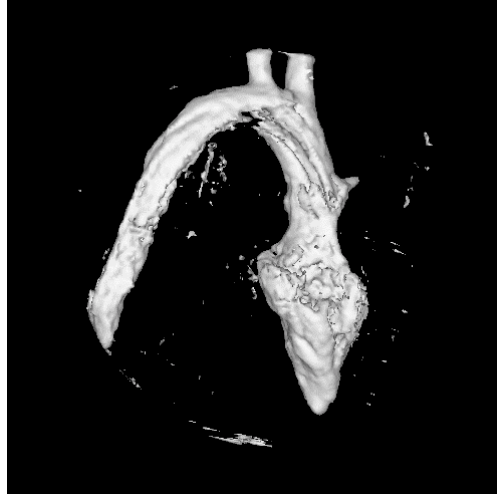


Fig. 3a

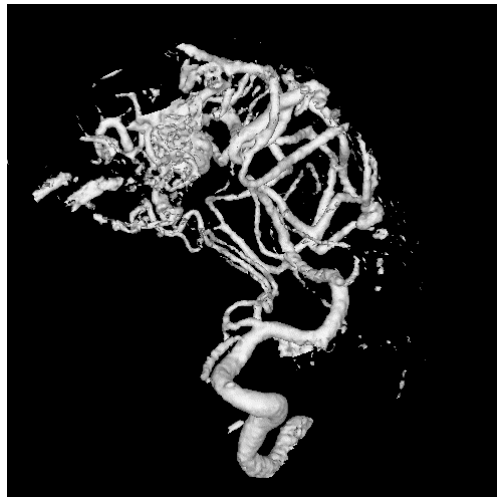


Fig. 3b

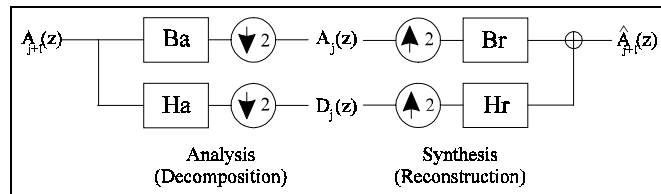


Fig. 4

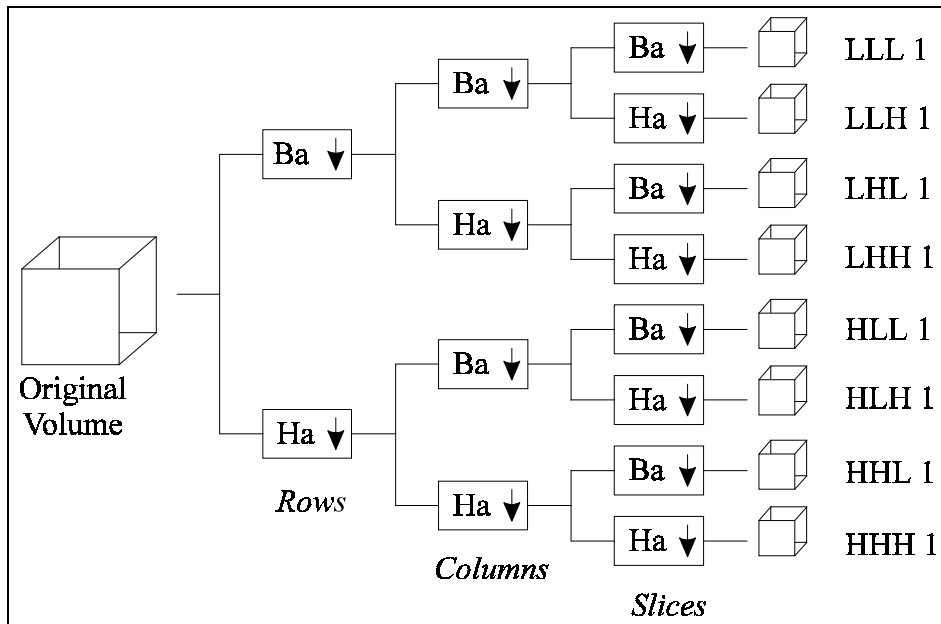


Fig. 5

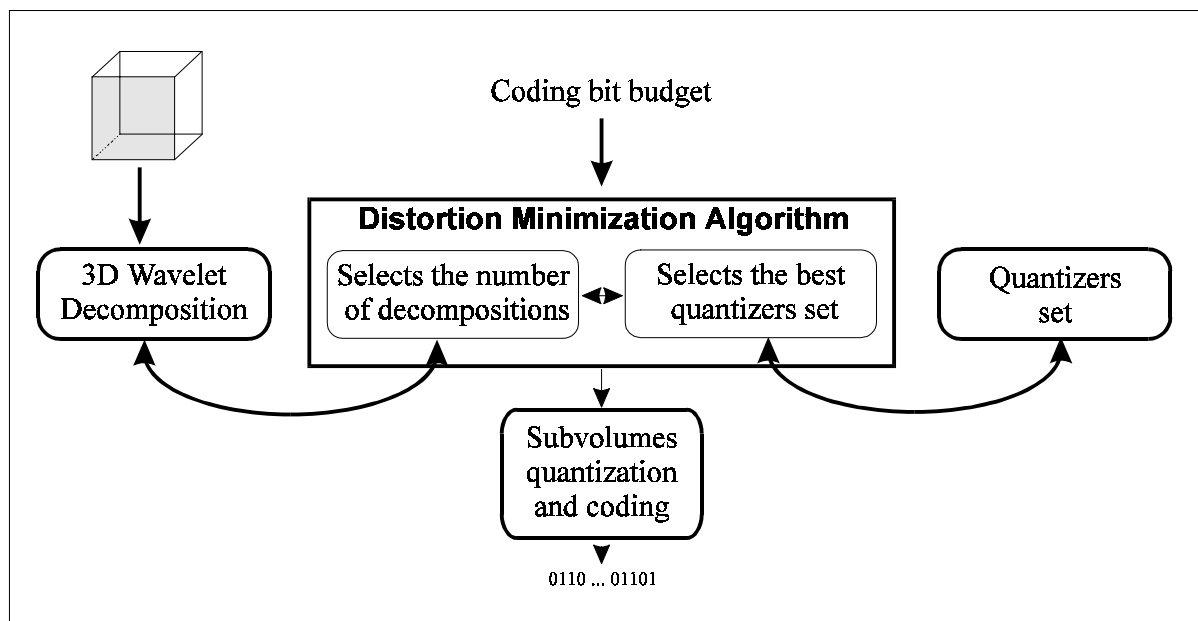


Fig. 6

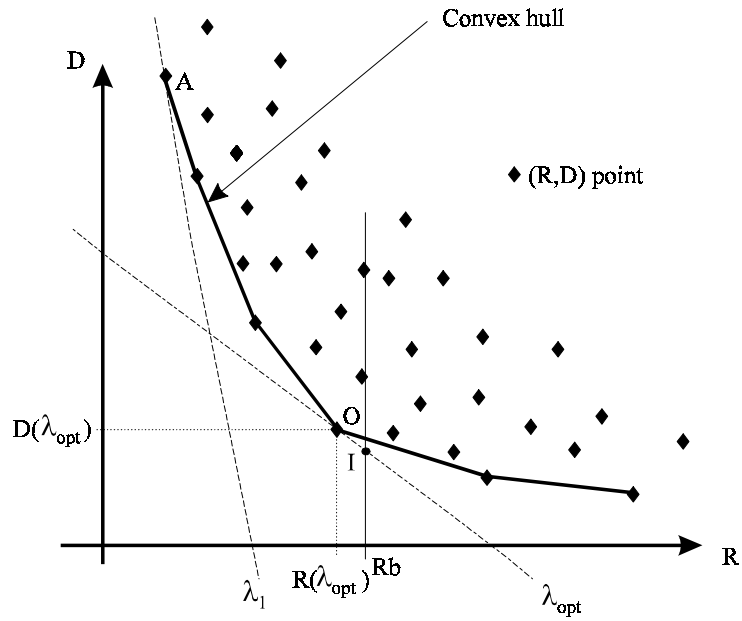


Fig. 7

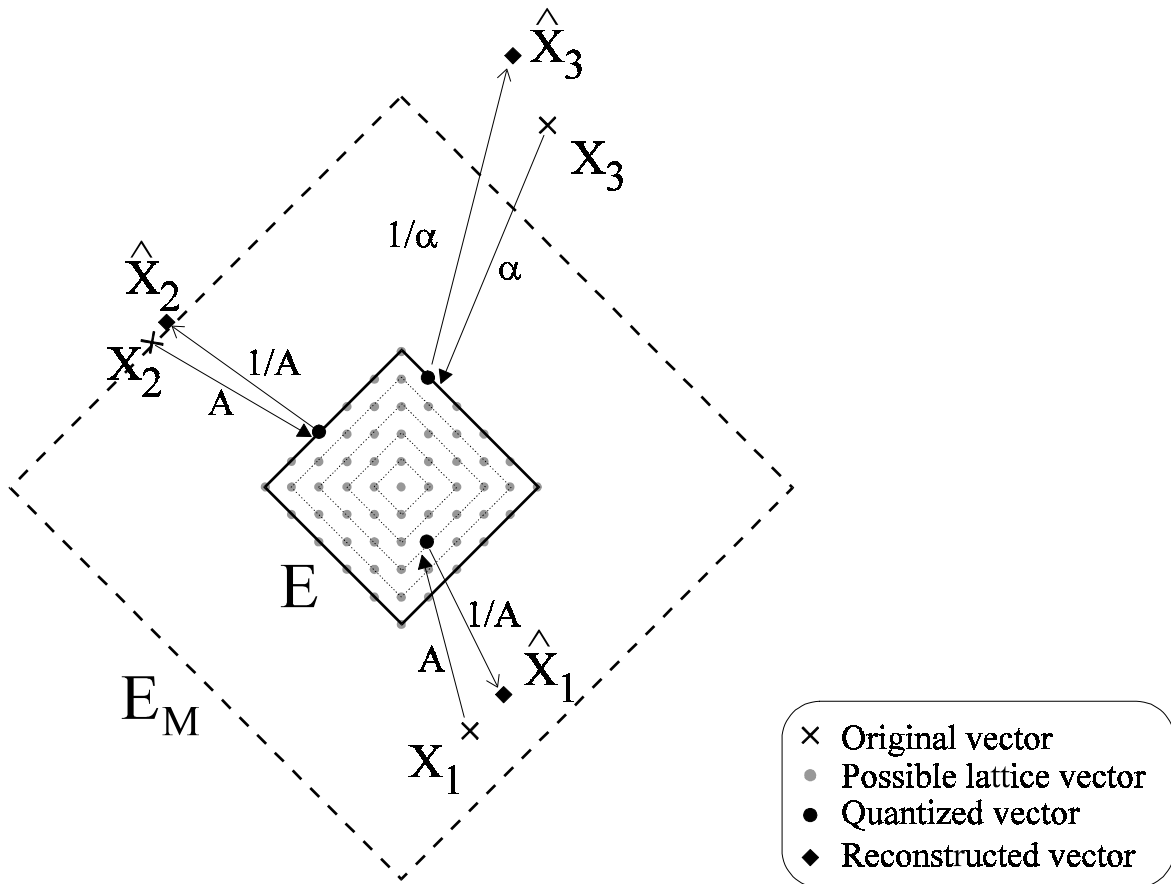


Fig. 8

- \times Original vector
- \bullet Possible lattice vector
- \bullet Quantized vector
- \diamond Reconstructed vector

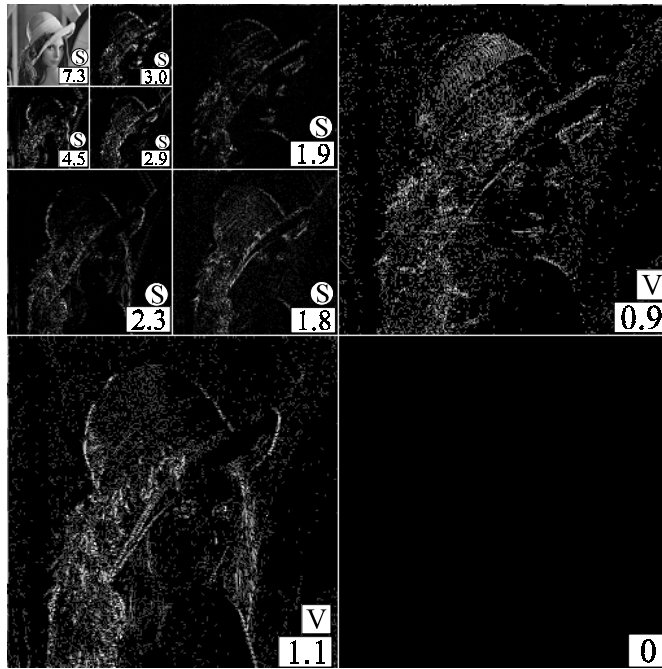


Fig. 9

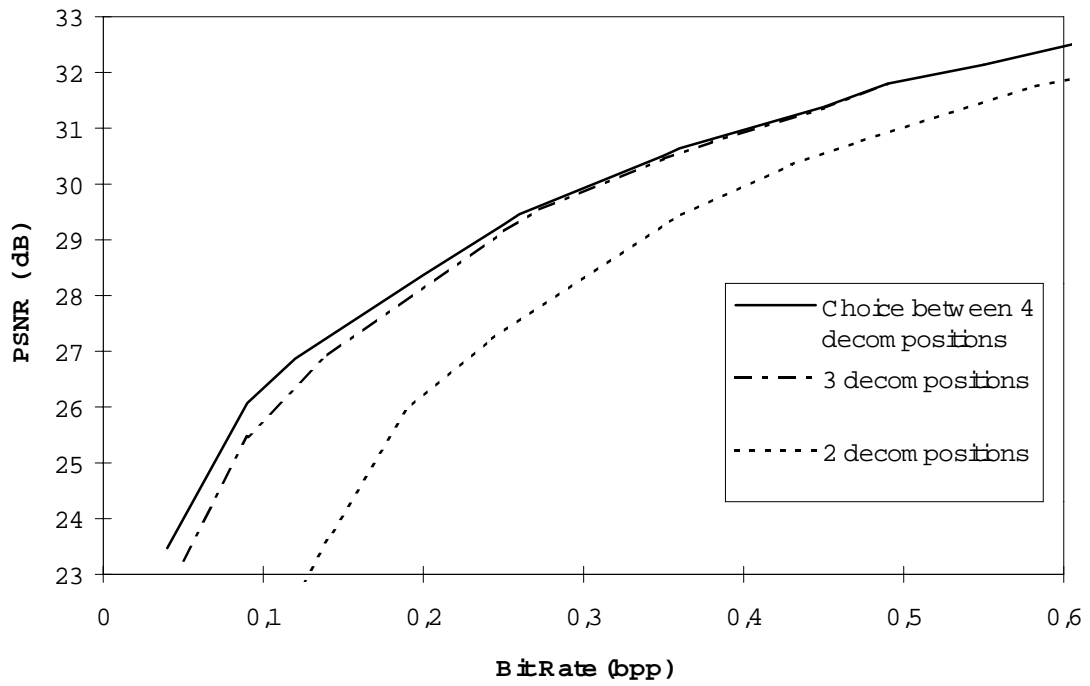


Fig. 10



Fig. 11a



Fig. 11b

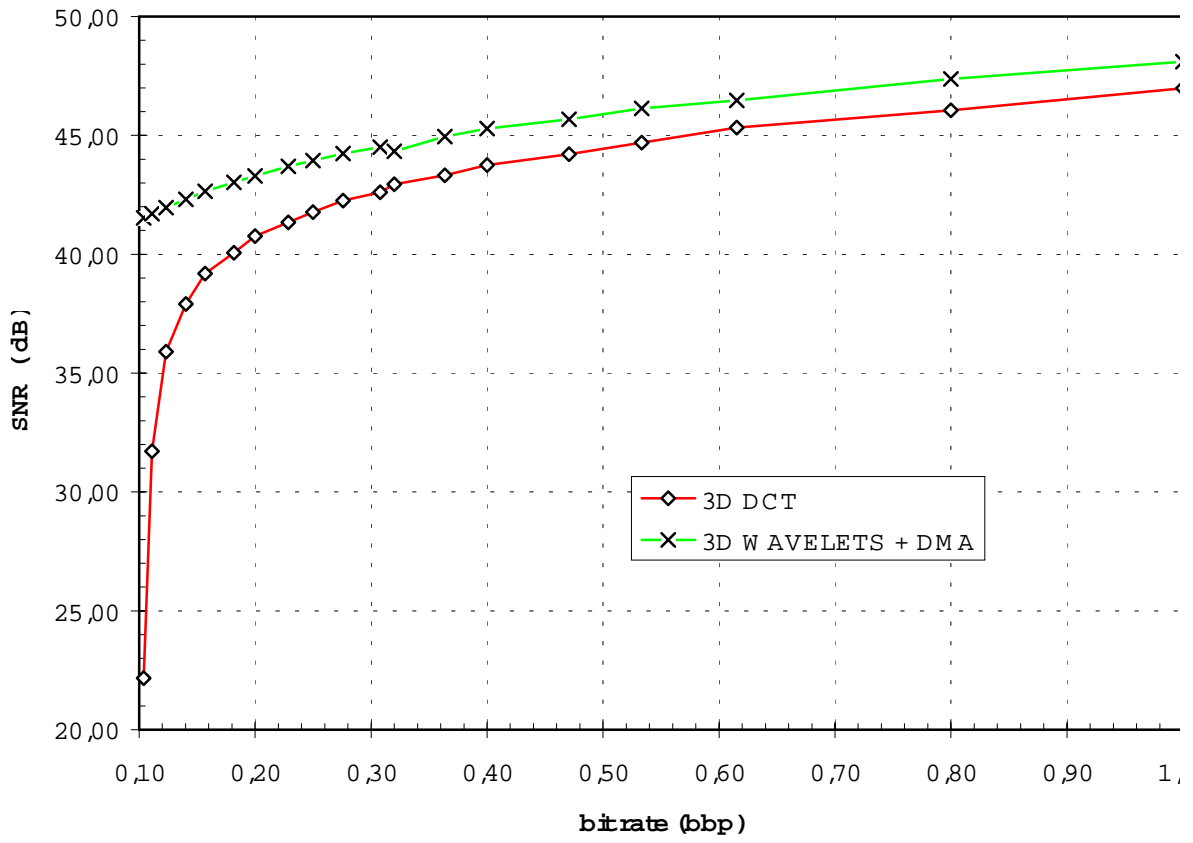


Fig. 12

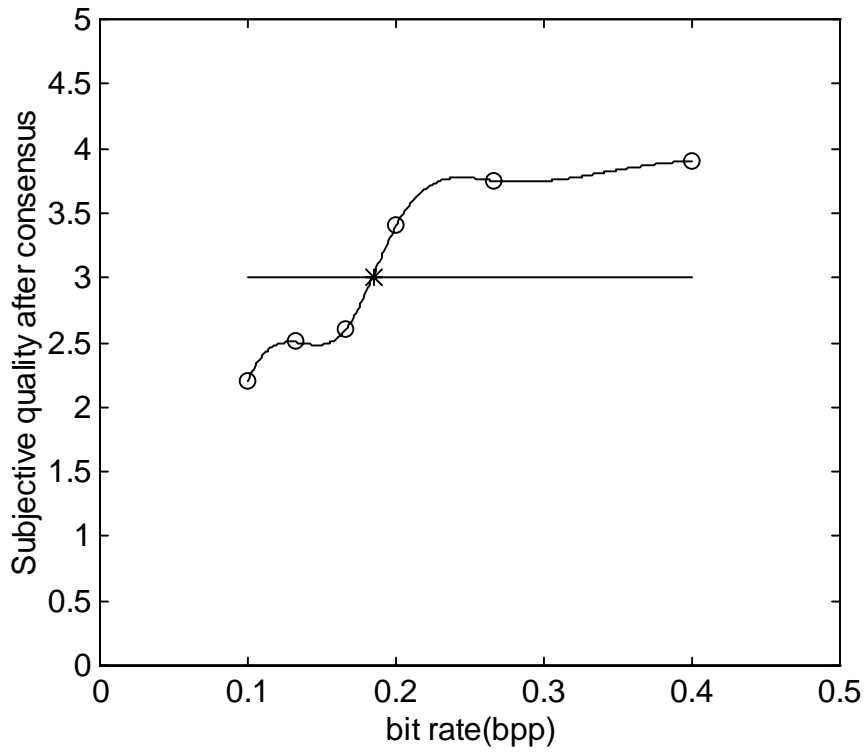


Fig. 13

Resolution number	LLL	LLH	LHL	LHH	HLL	HLH	HHL	HHH
0	-	-	-	-	-	-	-	-
1	-	1.3	1.2	0	1.2	0	0	0
2	-	1.8	1.7	1.5	1.7	1.4	1.5	1.4
3	3.5	2.8	3.3	2.8	3.2	2.7	2.9	2.2

Table 1

Resolution number	LLL	LLH	LHL	LHH	HLL	HLH	HHL	HHH
0	-	-	-	-	-	-	-	-
1	-	V:0.5	V:0.8	V:0.6	V:0.6	V:0.4	V:0.5	V:0.5
2	-	S:2.1	S:2.0	V:1.0	S:1.9	V:1.0	S:1.7	V:1.1
3	S:5.7	S:3.5	S:3.3	S:2.8	S:3.2	S:2.7	S:2.9	V:1.9

Table 2